Supporting Online Material for

Anti-Hebbian Long-Term Potentiation in the Hippocampal Feedback Inhibitory Circuit

Karri P. Lamsa, Joost H. Heeroma, Peter Somogyi, Dmitri A. Rusakov, Dimitri M. Kullmann*

*To whom correspondence should be addressed. E-mail: d.kullmann@ion.ucl.ac.uk

Published 2 March 2007, *Science* **315**, 1262 (2007)
DOI: 10.1126/science.1137450

This PDF file includes:

Supporting Online Material

Materials and Methods

Three to four week old male Sprague-Dawley rats were sacrificed according to the Animals (Scientific Procedures) Act 1986. Hippocampal slices (300 – 350 μm thick) were visualized with infra-red differential interference contrast and epifluorescence imaging. A cut was made between CA1 and CA3 to prevent propagation of recurrent excitation in Schaffer collaterals. The perfusion medium contained (in mM): NaCl (119), KCl (2.5), $MgCl_2$ (1.3), $CaCl_2$ (2.5), $NaHCO_3$ (25), NaH_2PO_4 (1), glucose (11), equilibrated with 95% O_2: 5% CO_2 (pH 7.4, 31 – 32^o C). The GABA receptor blockers picrotoxin (100 μM) and CGP52432 (5 μM) were routinely added to the solution (except in Figs. 1 and 2 and figs. S1 and S6).

Electrical stimuli (50 μs, 50 – 500 μA) were delivered via bipolar stainless steel electrodes in the *alveus*, with a 15 – 20 s inter-trial interval during baseline and after LTP induction. Cells were recorded with a Multiclamp 700 amplifier (Molecular Devices).

Perforated patch recordings were made with 10 – 15 MΩ pipettes containing gramicidin (100 μg/ml) in a solution containing (in mM): K-gluconate (145), NaCl (8), KOH-HEPES (20 – 25), EGTA (0.2), and QX-314 Br (5) (pH 7.2, 295 mOsm). The electrode tip was filled with gramicidin-free solution. Series resistance was continuously monitored throughout the experiment, and recordings in bridge balance mode were started when it was <100 MΩ. Depolarizing currents were intermittently injected to evoke action potentials to verify patch integrity. In some experiments QX-314 was omitted and 20 μM Alexa Fluor 488 was included, and the neuron was imaged with epifluorescence to monitor dye penetration. If the patch ruptured spontaneously the experiment was discontinued.

Evoked EPSPs were recorded from the resting membrane potential (liquid junction potential corrected), low-pass filtered (5 Hz) and acquired at 20 kHz on PC for off-line analysis (LabView, National Instruments). In some experiments EPSPs were recorded during a brief (500 ms) hyperpolarizing step (5 – 10 mV) to avoid action potential generation. The initial slope (range 3 – 7 ms from onset) of the EPSPs was measured, and in the LTP experiments all EPSPs were visually

verified to restrict attention to monosynaptic excitatory inputs. (Analyzing the peak slope during the same interval gave similar results.)

In the experiments illustrated in Fig. 1 the baseline EPSP amplitude of the 'weak' pathways was 3.1 ± 1.7 mV (Fig. 1A), 2.8 ± 0.2 mV (Fig. 1C), and 3.4. ± 0.7 mV (Fig. 1E). High-frequency burst (HFB) stimulation consisted of brief 5-pulse trains at 100 Hz. Five HFBs were delivered at 4 – 5 Hz, and this was repeated 4 times, with 10 s pauses between groups of HFBs (100 pulses in total). During anti-phase pairing (Fig. 1C) the somatic membrane potential was -58.6 ± 3.0 mV, compared to a resting value of -65.2 ± 1.6 mV. For low-frequency stimulation the same total number of stimuli (100) was given at 1 or 5 Hz, as indicated. High-frequency tetanic stimulation (HFS) consisted of 100 pulses at 100 Hz, delivered twice with a 10 s pause.

For the experiments illustrated in Fig. 2 the imposed somatic voltage oscillation was designed to give a trough membrane potential of -90 mV, which is likely to overestimate the dendritic hyperpolarization because of electrotonic attenuation (*1*).

Whole cell voltage-clamp recordings were made with a solution containing (in mM): Cs-gluconate (117.5), CsCl (17.5), KOH-HEPES (10), BAPTA (10), NaCl (8), Mg-ATP (2), GTP (0.3), spermine tetrahydrocholride (0.1) and QX-314 Br (5) (pH 7.2, 290 mOsm). Biocytin or neurobiotin (0.4%) was included in most experiments. Cells showing unstable series resistance or holding current were rejected. Because NMDAR-mediated signaling rapidly washes out when interneurons in *stratum radiatum* are recorded in whole cell mode (*2*) we measured the *I-V* relationship for NMDAR-mediated EPSPs within 5 minutes of breaking in. The AMPAR-mediated EPSC rectification index was obtained by dividing the amplitude of the EPSC recorded at +60 mV by that predicted from linear extrapolation of the current-voltage (*I-V*) relationship measured at negative potentials. For this extrapolation, the regression line was taken from EPSCs (mean of ≥ 4 at each point) at -90mV, -60 mV, and -30 mV. The NMDA/AMPA ratio was calculated by dividing the amplitude of the late outward NMDAR-mediated EPSC at +60 mV by the amplitude of the early inward AMPAR-mediated EPSC at -60 mV. The early and late time points were ≤ 5ms and 50 ms from EPSC onset, respectively. (We have not discriminated between AMPA and kainate receptors with selective blockers in this study. Therefore we cannot exclude a contribution of Ca^{2+}-permeable kainate receptors, although their slower kinetics (*3*) make it unlikely that they contribute substantially to the early EPSC used to measure rectification.) For the whole-cell current-clamp experiments illustrated

in Fig. 4, K-gluconate was used instead of Cs-gluconate, and the spermine concentration, where added, was 1 mM. Series resistance (<20 MΩ) was monitored throughout the experiment using a -5 or -10 mV step command. In Fig. 4, seal test steps (-10 mV) were run also during the pairing protocol (see insets in Fig. 4D - F).

Although repetitive synaptic activity attenuates polyamine blockade of CP-AMPARs (*4*), HFB stimulation did not prevent rectification of *alveus*-evoked EPSCs in 5 interneurons in *stratum oriens* when recorded with a whole-cell pipette solution containing as little as 100 μM spermine (data not shown). Endogenous polyamines have been estimated to be equivalent to this concentration or higher (*5, 6*).

For cell identification, a whole-cell recording was obtained from the same cell with a pipette containing 0.4% neurobiotin, biocytin, or biocytin conjugated to the fluorescent dye Alexa Fluor 488. Slices were fixed overnight in 4% paraformaldehyde at 4 C˚. After permeabilization in 0.1% TritonX-100, slices were incubated in 0.1% streptavidin-Cy3 conjugate, mounted in DABCO anti-fading medium. Cells were first imaged with a confocal microscope to record the dendritic and axonal patterns, whereupon the slices were incubated in a solution of avidin-biotinylated horseradish peroxidase (HRP) complex in Tris-buffered (TB) saline, containing 0.3% Triton. Peroxidase activity was visualized by incubation for 5 min in 0.05% 3,3'–diaminobenzidine tetrahydrochloride (DAB) in TB (pH 7.6) followed by another 10 min in DAB containing 0.01% H_2O_2. After more extensive washing, first in TB, then in 0.1 M phosphate buffer (PB), slices were treated with 1% OsO_4 in 0.1 M PB for 1 hour before they were washed in PB, dehydrated, and finally permanently mounted in Durcupan resin on glass slides under a coverslip.

Data are shown as mean ± s.e.m., normalized by baseline values. Significance was analyzed with Student's paired t-test. In order to estimate the magnitude of LTP the change in EPSP initial slope for the paired pathway was corrected for minor drift in the unpaired control pathway, according to the formula LTP = ($paired_2$/$paired_1$) ÷ ($control_2$/$control_1$), where the subscripts 1 and 2 refer to EPSP slopes measured before and after pairing, respectively. This gave the following values. Fig. 2A: 79 ± 15 % increase in EPSP initial slope when paired with hyperpolarization (n = 8), and 3 ± 10 % when paired with depolarization. Fig. 2C (all 10 cells paired with hyperpolarization): 36 ± 12 %. Fig. 2D (all 10 cells paired with depolarization): -6 ± 5 %. Fig. 3A (25 cells exhibiting LTP, measured 20-25 min after pairing): 64 ± 6 % (the other 6 cells showed no change). Fig. 4A: 87 ± 11

% (20 minutes after pairing) when paired with hyperpolarisation, and 13 ± 6 % when paired with depolarisation. Fig. 4B: 57 ± 7 % (1st pathway paired with hyperpolarisation), 12 ± 6 % (2nd pathway paired with depolarization), and 52 ± 6 % (paired with hyperpolarisation). Fig 4D: 42 ± 3 % (first pathway paired in perforated patch mode), 55 ± 5 % (second pathway paired in whole cell mode). Fig. 4E: 67 ± 10 % (1st pathway paired in perforated patch mode). Fig. 4F: 83 ± 7 % (1st pathway in perforated patch mode), 81 ± 5 % (second pathway in whole cell mode).

Fig. S1. Anti-Hebbian LTP occurs at synapses made by pyramidal cell axons on interneurons in *oriens-alveus* but is rare at synapses made by Schaffer collaterals on interneurons in *stratum radiatum.*

(A) High-frequency (100 Hz) burst (HFB) stimulation of the *alveus*, paired with the trough of an imposed postsynaptic sinusoidal membrane potential oscillation ("anti-Hebbian pairing"), induced pathway-specific LTP in 8 out of 11 interneurons *in stratum (s.) oriens-alveus*. **A_1** Schematic showing arrangement of recording (perforated patch) and stimulating electrodes. **A_2** Time-course of EPSP initial slopes in both pathways (mean ± s.e.m., n = 8, replotted from Fig. 2). LTP was not seen when stimulation of the other *alveus* pathway was paired with postsynaptic depolarization. **A_3** Two interneurons did not exhibit any potentiation following either pairing protocol. **A_4** One interneuron exhibited LTP following Hebbian but not anti-Hebbian pairing. **(B)** Pie chart showing the proportion of interneurons in each class. **(C)** Anti-Hebbian HFB did not elicit LTP at Schaffer collateral synapses onto interneurons in *stratum radiatum*. **C_1** Schematic illustrating experimental design. Instead, 6/11 interneurons exhibited LTP following Hebbian pairing (**C_2**). **C_3** The other five interneurons did not exhibit LTP with either protocol. **(D)** Summary pie chart. **(E)** Results of pairing single stimuli at 5 Hz with the trough (anti-Hebbian) or peak (Hebbian) of the somatic membrane potential oscillation in interneurons in *s. radiatum*. **E_1** Schematic showing experimental design. **E_2** Pairing with hyperpolarization (anti-Hebbian) failed to induce LTP (all 10 cells tested included in plot). **E_3** Pairing with depolarization (Hebbian) induced LTP (all cells included).

Although the term 'anti-Hebbian' has previously been used to describe long-term depression triggered by Hebbian pairing, we have used the term 'anti-Hebbian LTP' here to denote an increase in synaptic strength triggered by presynaptic activity and blocked by postsynaptic depolarization. It is induced by brief trains of presynaptic action potentials when the postsynaptic membrane potential is at rest, or by single action potentials when the membrane is hyperpolarized. We are aware of only one example of LTP with an anti-Hebbian induction rule in cerebellar nuclei (*7*), although this depends on NMDARs and also requires a rebound depolarization following the pairing. In contrast, anti-Hebbian LTP reported here depends on rectifying CP-AMPARs.

Fig. S2. Hebbian LTP occurs in interneurons with non-rectifying AMPARs and large NMDAR-mediated EPSCs.

(A) Pairing 1 Hz stimulation with depolarizing voltage commands failed to evoke LTP in all 12 tested interneurons in *s. oriens/alveus.* (LTP was elicited in one displaced pyramidal cell identified following re-patching in whole cell mode and *post hoc* visualization, which has been excluded.) **A_1** Schematic showing experimental design, and sample trace obtained in one cell during pairing (I_m), showing a train of escape currents. **A_2** Mean EPSP initial slope for 12 cells tested (pairing at time indicated by arrow). **A_3** Baseline-normalised EPSP initial slopes in paired and control pathways plotted against one another. Insets: averaged EPSPs in both pathways, recorded at times indicated in one cell. **(B)** Re-patched interneurons mainly showed highly rectifying synaptic AMPARs and a small NMDAR-mediated component. **B_1** Rectification indices for paired and unpaired pathways in 6 re-patched interneurons. **B_2** NMDA/AMPA ratio in 5 cells. (The NMDAR-mediated component could not be reliably measured in one further cell.) Sample traces: EPSCs measured at +60 mV and -60 mV, respectively (scale-bars 50 pA / 50 ms), in both pathways. **B_3** The re-patched interneurons were visualized *post hoc*. Three were identified as O-LM cells, one of which is shown with axon in blue and somatodendritic structures in red (Scale: 200 μm). Three further cells had horizontal dendrites but axons were not visualized. **(C)** Hebbian LTP was induced in 17 out of 37 interneurons in *stratum radiatum*. **C_1** Schematic showing experimental design and sample traces during pairing in one cell. **C_2** Top: Mean EPSP initial slope for 17 cells showing LTP of the paired pathway (filled symbols). Bottom: 20 cells not showing LTP. **C_3** EPSP slopes plotted as in A_3. Gray symbols: cells showing pathway-specific LTP. Inset; averaged EPSPs before (-10 min) and after (20 min) LTP induction in one cell. **(D)** Re-patched interneurons in *stratum radiatum* exhibiting Hebbian LTP had non-rectifying AMPARs and large NMDAR-mediated EPSCs. **D_1** AMPAR-mediated EPSC *I-V* relationship obtained from 9 re-patched cells expressing Hebbian LTP. **D_2** EPSCs in the potentiated and un-paired pathways show similar rectification profiles. Gray symbols: cells exhibiting Hebbian LTP. **D_3** *I-V* relationship of the NMDAR-mediated component in cells showing Hebbian LTP. **D_4** NMDA/AMPA ratio. The symbols for the cells showing LTP fall above the line of identity, consistent with a relatively selective increase in the AMPA component. Inset; averaged EPSCs at -60 and +60 mV. Scale-bars 50 pA / 50 ms. **D_5** Soma and dendrites of an interneuron showing Hebbian LTP (scale: 200 μm). The axon was not recovered and further identification was therefore not possible. GABA receptors were blocked in all experiments.

Fig. S3. NMDAR-independent LTP is rare at Schaffer collateral synapses on interneurons in s. *radiatum*.

(A) Top: Schematic showing experimental design. SC1, SC2: Schaffer collateral pathways. Bottom: Pairing high-frequency afferent stimulation (100 Hz 1s, twice) with postsynaptic depolarization in the presence of the NMDAR antagonist APV (100 μM) failed to induce pathway-specific potentiation lasting >10 min in any of 20 cells studied (filled symbols). Open symbols indicate the unpaired control pathway. Right: averaged EPSPs in one cell in both pathways before and after pairing. **(B)** Results of pairing high-frequency stimulation with postsynaptic hyperpolarization in 20 cells. Right: traces from one cell. **(C)** Baseline-normalised EPSP slopes in the tetanized and control pathways plotted against one another 15 min following the pairing. NMDAR-independent LTP was elicited in only two out of 40 attempts (gray symbols). The 40 pairings were perfomed in 17 interneurons in *stratum radiatum* where two pathways were tested, and 6 cells where only one pathway was tested, with either depolarization or hyperpolarization. **(D)** Re-patching 11 interneurons, none of which exhibited LTP, revealed weakly or non-rectifying AMPAR-mediated EPSCs. The histogram shows the distribution of the EPSC rectification indices in all 22 pathways. Inset; averaged EPSCs from one re-patched interneuron, recorded at -60mV and +60 mV. The two interneurons that showed anti-Hebbian LTP were not successfully re-patched. However, rectifying AMPAR-mediated EPSCs were recorded in 4 fast-spiking interneurons in *stratum pyramidale* when stimulating in *stratum radiatum* (see fig. S6). GABA receptors were blocked in all experiments.

Fig. S4. Electrophysiological characterization of all interneurons recorded with perforated patch clamp following the Petilla convention (*8*) (http://www.columbia.edu/cu/biology/faculty/yuste/petilla/)

Interneurons were divided into 7 categories according to their passive and firing properties: regular-spiking non-pyramidal cells (RSNP), classified further as rebounding (R-), non-rebounding (NR-), and rapidly adapting (RA-) RSNPs; burst-spiking nonpyramidal cells (BSNP); fast-spiking interneurons (FS); irregularly-spiking interneurons (IS); delayed spiking interneurons (DS). **(A)** FS interneurons. $\mathbf{A_1}$ FS interneurons were either non-rebounding (left) or rebounding (right). Rebounding interneurons generated action potentials (arrow) on release from hyperpolarizing current injection (to -90 mV). Interneurons in this class were recorded in *stratum oriens* and *s. pyramidale.* $\mathbf{A_2}$ These cells had a high maximal spiking frequency and small reduction in the spiking frequency when comparing initial (0-100 ms) and later (400-500 ms) periods. **(B)** R-RSNP cells. $\mathbf{B_1}$ Representative R-RSNPs in *stratum oriens* (left) and *stratum radiatum* (right). Rebounding action potentials indicated by arrow. $\mathbf{B_2}$ RSNPs showed spike frequency adaptation during maximal spiking. **(C)** NR-RSNP cells. $\mathbf{C_1}$ NR-RSNPs in *stratum oriens* (left) and *stratum radiatum* (right). $\mathbf{C_2}$ as above. **(D)** RA-RSNP cells. $\mathbf{D_1}$ RA-RSNPs in *stratum oriens* and *stratum radiatum*. These cells showed initially regular spiking behaviour, which stopped after a few hundred milliseconds during maximal spiking. $\mathbf{D_2}$ as above. **(E)** BSNP cells. $\mathbf{E_1}$ Representative BSNP-type interneurons recorded in both strata. These cells characteristically generated high-frequency bursts of action potentials (≥3) on release from hyperpolarizing current injection. $\mathbf{E_2}$ as above. **(F)** IS cells. $\mathbf{F_1}$ In IS interneurons spiking was irregular and intermittent even during their maximal spiking frequency. $\mathbf{F_2}$ as above. **(G)** DS cells. $\mathbf{G_1}$ DS interneuron recorded in *stratum radiatum*. $\mathbf{G_2}$ as above.

Fig. S5. Electrophysiological properties of interneurons showing anti-Hebbian LTP.

Box plots comparing active and passive membrane properties of re-patched interneurons and all fast-spiking cells that showed anti-Hebbian LTP (electrophysiological properties recorded in perforated patch). Cells were categorized as: O-LM (anatomically identified O-LM cells, n = 7); horizontal (cells with horizontal dendrites similar to those of the identified O-LM cells, but with insufficient axon visualization, n = 12); fast spiking (fast-spiking interneurons, which characteristically showed little spike frequency adaptation, n = 17); other (anatomically unidentified, firing pattern not fast-spiking, n = 7). The data suggest that anti-Hebbian LTP is not restricted to O-LM and fast-spiking interneurons contributing to the feedback inhibitory circuitry.

Maximal firing frequency was taken from the first 100 ms during maximal action potential firing generated by a >500 ms depolarizing step. Firing adaptation (%) was obtained by comparing the initial 0-100 ms and subsequent interval 400-500 ms following injection of a current giving a maximal firing frequency. The delay to spike represents an average latency to the first spike for three or more depolarizing steps slightly above the firing threshold. Afterhyperpolarization (AHP) amplitude was measured from the first action potential initiated during the delay-to spike test. Input resistance (Rin) was measured using a -100 pA (1 s) current pulse. Em, resting membrane potential. Membrane time constant (Tau) was determined from the negative slope of a -10 mV step at resting membrane potential. V-sag was measured from a hyperpolarizing step to -90 mV.

Fig. S6. Evidence for target-cell dependent properties of synapses made by Schaffer collaterals on inhibitory interneurons.

Excitatory currents evoked by stimulating in *stratum radiatum* (to activate Schaffer collaterals) and in the *alveus* (to stimulate CA1 pyramidal cell collaterals) were compared in fast-spiking interneurons in *stratum pyramidale*. These cells contribute to both feed-forward and feedback inhibition (*9*). **(A)** Fast-spiking GABAergic interneurons (recorded in perforated patch mode in *stratum pyramidale*) were identified by demonstrating that a presynaptic action potential evoked an inhibitory postsynaptic current in a local pyramidal neuron. A_1 Schematic showing experimental design. A_2 Simultaneously recorded presynaptic voltage and postsynaptic current traces in one interneuron (IN) – pyramidal cell (PC) pair. A_3 The presynaptic cells showed a fast-spiking pattern in response to depolarizing current injection with very little firing adaptation. **(B)** Monosynaptic EPSPs were then elicited in the interneuron by stimulation in the *alveus* and in the *stratum radiatum* (B_1 schematics) to activate Schaffer collaterals and CA1 pyramidal cell axon collaterals, respectively. We then paired *stratum radiatum* stimulation with depolarization of the interneuron (100 Hz 1s, delivered twice). This failed to elicit LTP in any of four cells. B_2 Baseline-normalized EPSP initial slopes (25 min following pairing) in the two pathways, plotted against one another. **(C)** The interneurons were re-patched with whole cell (**C_1**). **C_2** In contrast to Schaffer collateral-synapses onto interneurons in *stratum radiatum*, synaptic AMPARs in these cells showed strong rectification.

Fig. S7. NMDAR-independent LTP in interneurons in *oriens/alveus* is sensitive to group I metabotropic glutamate receptor (mGluR) blockade.

Top: schematic showing arrangement of stimulation and recording electrodes. (Experiments were carried out in interneurons in *oriens/alveus* with horizontal dendrites.) NMDA and GABA receptors were blocked throughout. Summary plot: EPSP initial slope showing LTP induced by pairing tetanic stimulation of one pathway with hyperpolarization (filled symbols, top). The group I mGluR antagonists LY367385 (100 μM) and 2-Methyl-6-(phenylethynyl)-pyridine (MPEP, 10 μM) were subsequently washed in and the second pathway (open symbols, bottom) was paired as above. This failed to evoke any potentiation.

Although this result confirms that group I mGluRs are necessary for LTP induction in interneurons in *oriens/alveus* (*10, 11*), the effects of manipulating the postsynaptic voltage and polyamines show that they are not sufficient. We cannot exclude the possibility that the threshold for induction of LTP is modulated by the degree of activation of mGluRs: high frequency presynaptic stimulation, which may have preferentially activated perisynaptic group I mGluRs, was required to induce LTP when the postsynaptic membrane potential was near its resting value (Fig. 1C,D), but low frequency stimulation was sufficient when interneurons were hyperpolarized (Fig. 2C). Whether they play the same role in different types of interneurons exhibiting anti-Hebbian LTP, which show distinct patterns of immunoreactivity for group I mGluRs (*12*), remains to be determined.

Fig. S8. Anti-Hebbian LTP was accompanied by an increased sensitivity to extracellular polyamines.

(A) LTP was evoked in 7 cells recorded in perforated patch mode by pairing tetanic stimulation of one pathway (filled symbols) with hyperpolarization to -90 mV. **(B)** Summary plot showing pathway-specific LTP. **(C)** *NHPP*-spermine (5 – 10 μM) was subsequently added to the perfusion solution. This caused a gradual decrease in EPSP slope, which was more rapid in the LTP pathway than in the control pathway. EPSP initial slopes are shown normalized to the value immediately prior to application of *NHPP*-spermine. **(D)** EPSPs in potentiated and control pathways, showing a significantly greater attenuation of the potentiated EPSP. EPSPs are shown normalized by the peak amplitude prior to adding *NHPP*-spermine. Scale-bar: 50 ms. NMDA and GABA receptors were blocked in all experiments.

These results, taken together with evidence that LTP in interneurons in *stratum oriens* is associated with decreases in failure rate and short-term facilitation (*10*), imply a presynaptic expression mechanism. Using a similar experimental design we looked for evidence that CB1 receptors are involved, because these have been implicated in retrograde signaling at other synapses in the hippocampus (*13*). The CB1 receptor blocker AM-251 (20 μM) however failed to prevent anti-Hebbian LTP induction (143 ± 37 % increase in EPSP slope, n = 4, data not shown).

Supplementary references

1. D. Thurbon, A. Field, S. Redman, *J Neurophysiol* **71**, 1948 (1994).
2. K. Lamsa, J. H. Heeroma, D. M. Kullmann, *Nat Neurosci* **8**, 916 (2005).
3. R. Cossart *et al.*, *Neuron* **35**, 147 (2002).
4. A. Rozov, N. Burnashev, *Nature* **401**, 594 (1999).
5. D. Bowie, M. L. Mayer, *Neuron* **15**, 453 (1995).
6. S. D. Donevan, M. A. Rogawski, *Proc Natl Acad Sci U S A* **92**, 9298 (1995).
7. J. R. Pugh, I. M. Raman, *Neuron* **51**, 113 (2006).
8. R. Yuste, *Neuron* **48**, 524 (2005).
9. L. L. Glickfeld, M. Scanziani, *Nat Neurosci* **9**, 807 (2006).
10. V. Lapointe *et al.*, *J Physiol* **555**, 125 (2004).
11. Y. Perez, F. Morin, J. C. Lacaille, *Proc Natl Acad Sci U S A* **98**, 9401 (2001).
12. F. Ferraguti *et al.*, *Hippocampus* **14**, 193 (2004).
13. R. I. Wilson, R. A. Nicoll, *Nature* **410**, 588 (2001).

Lamsa *et al*. Fig. S1

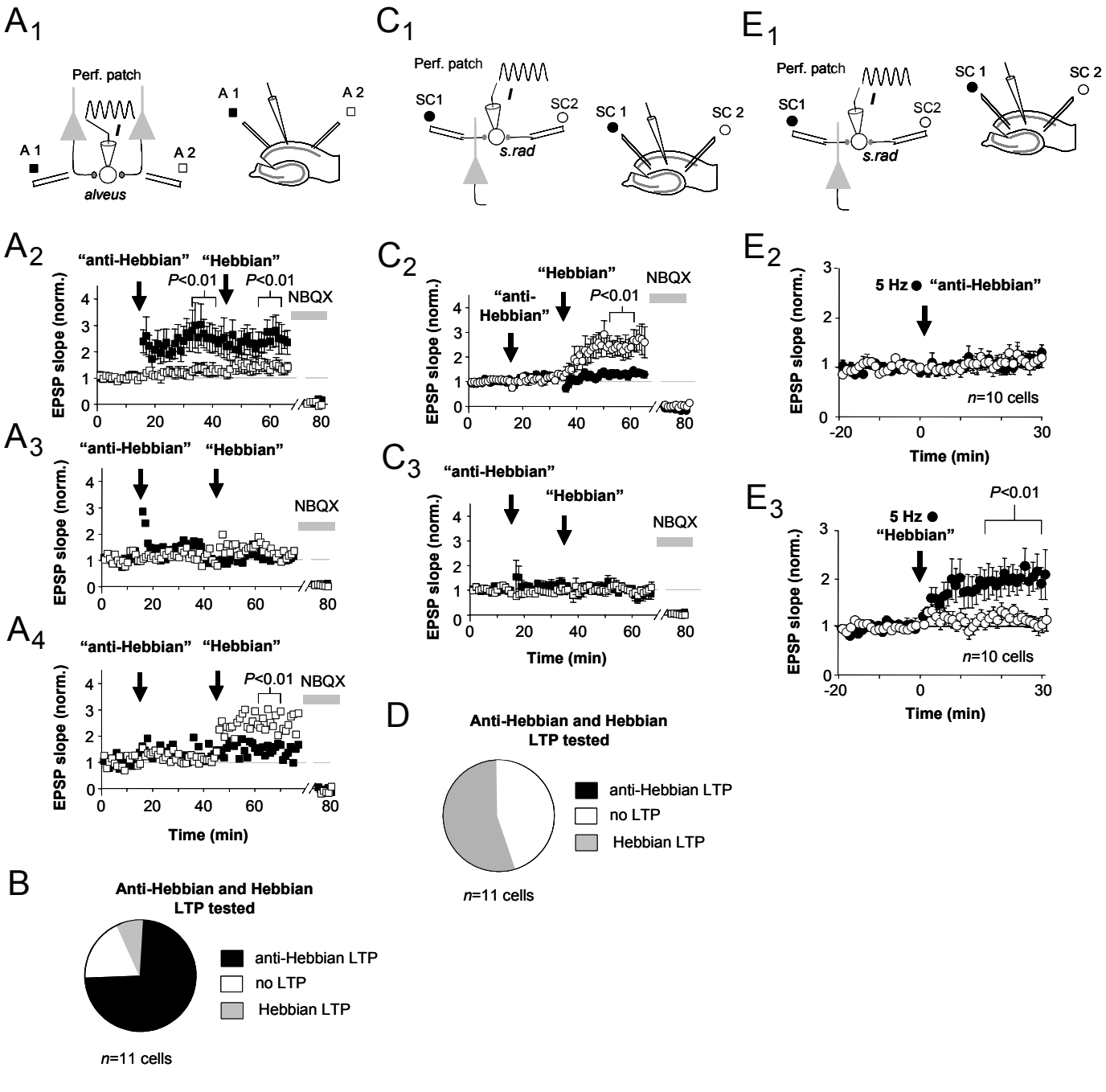

Lamsa *et al*. Fig. S2

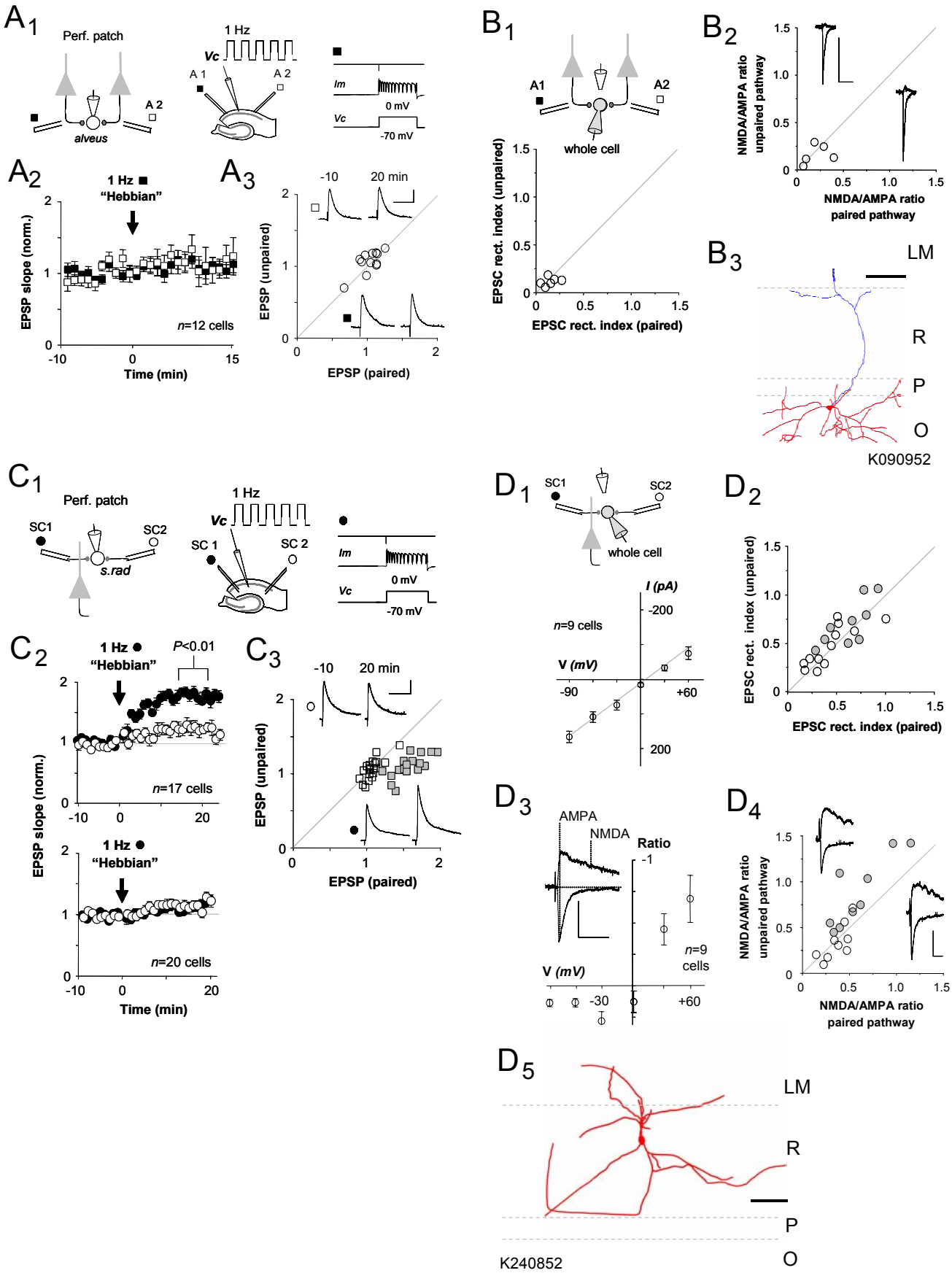

Lamsa *et al*. Fig. S3

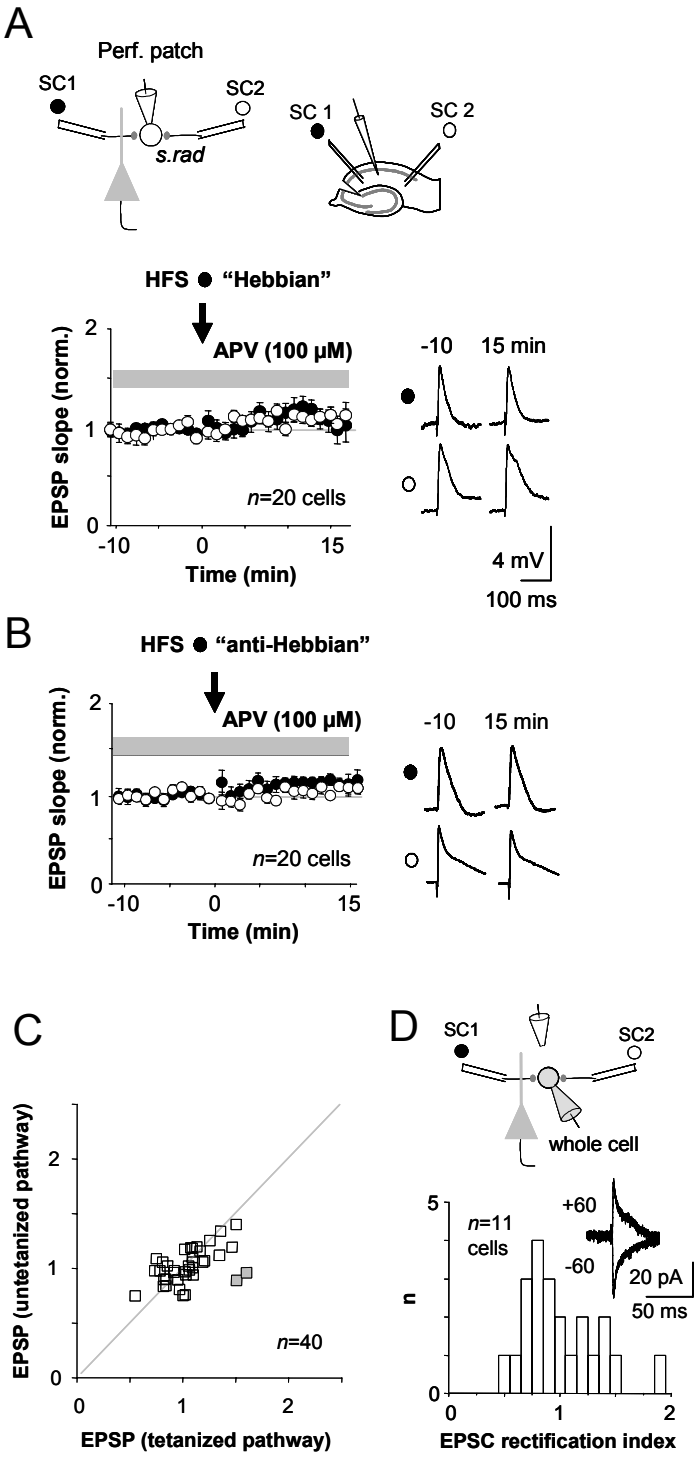

Lamsa *et al*. Fig. S4A-D

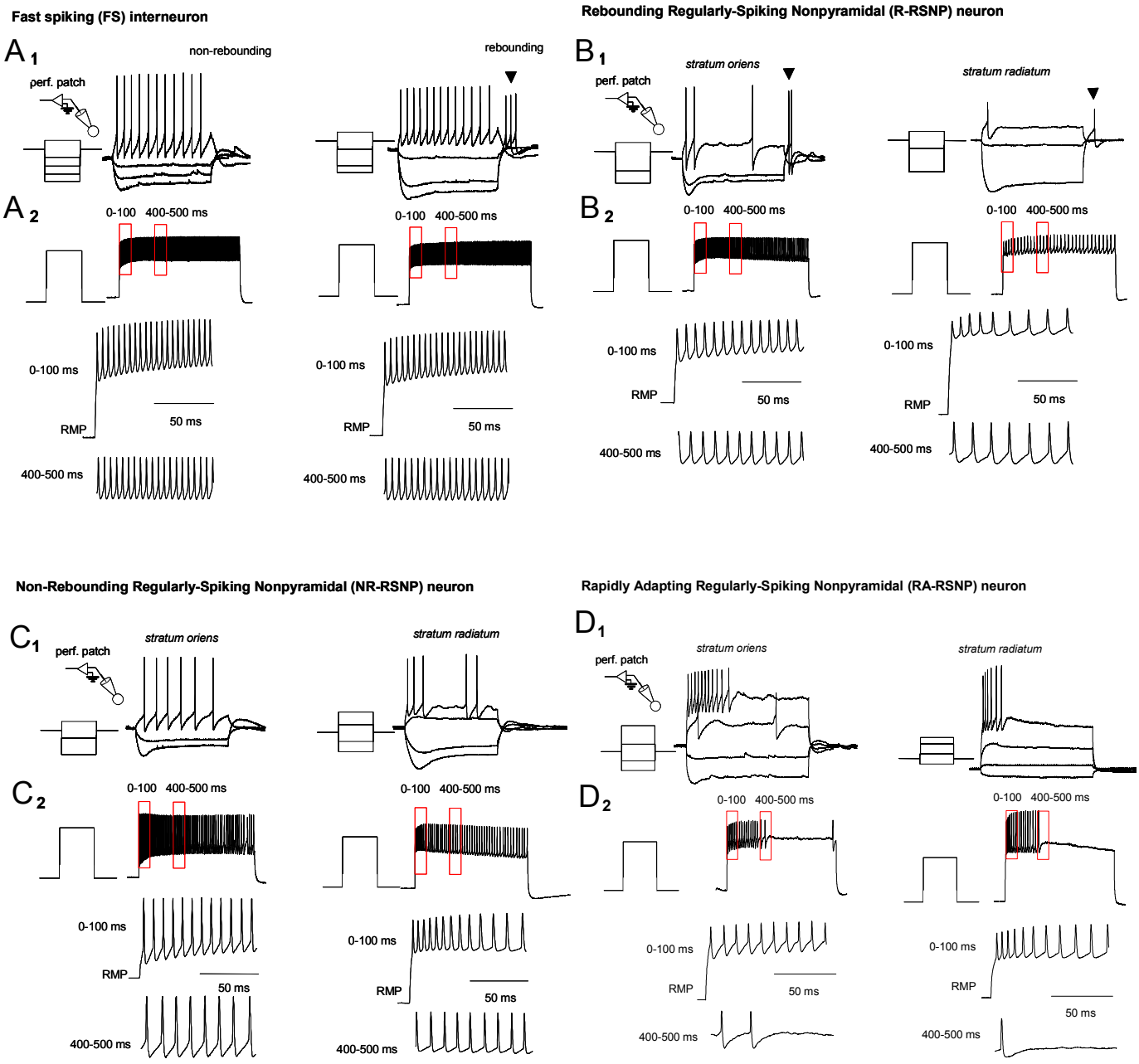

Lamsa *et al*. Fig. S4E-G

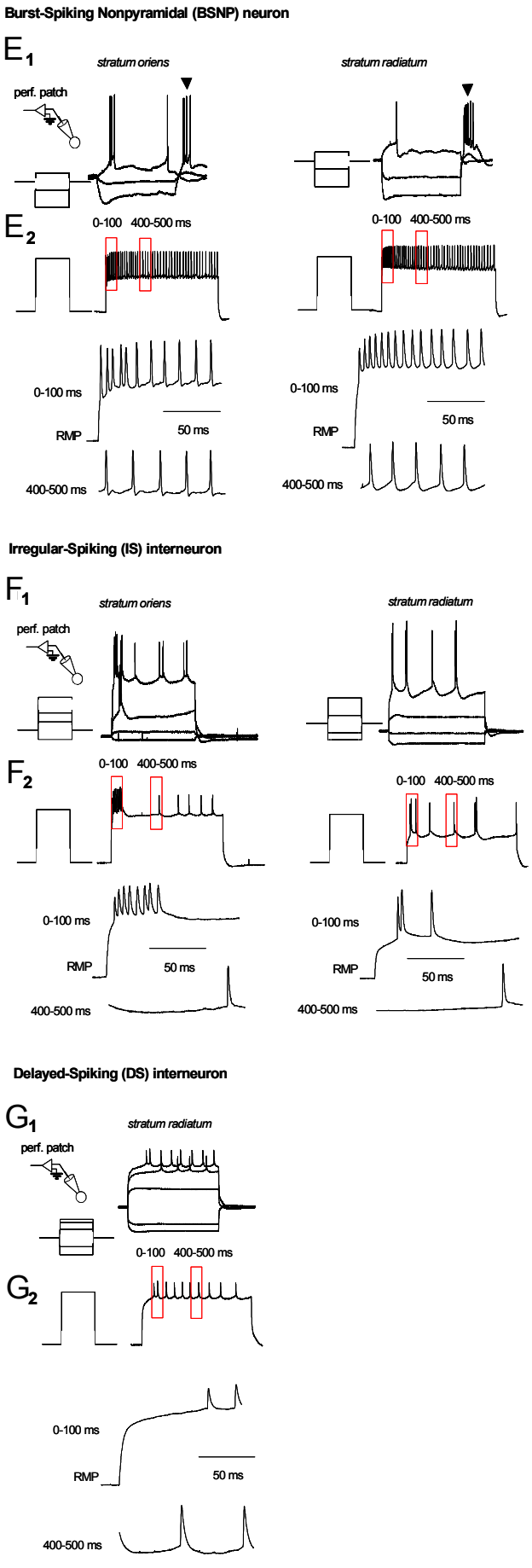

Lamsa *et al*. Fig. S5

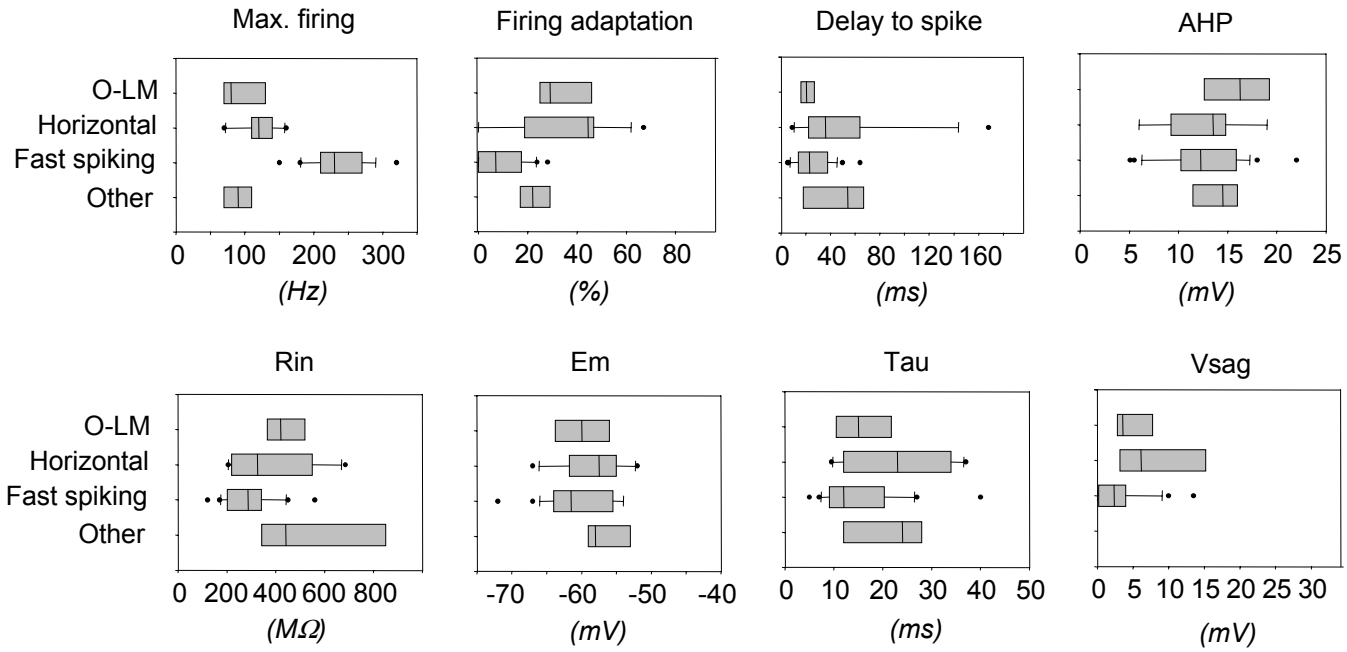

Lamsa *et al*. Fig. S6

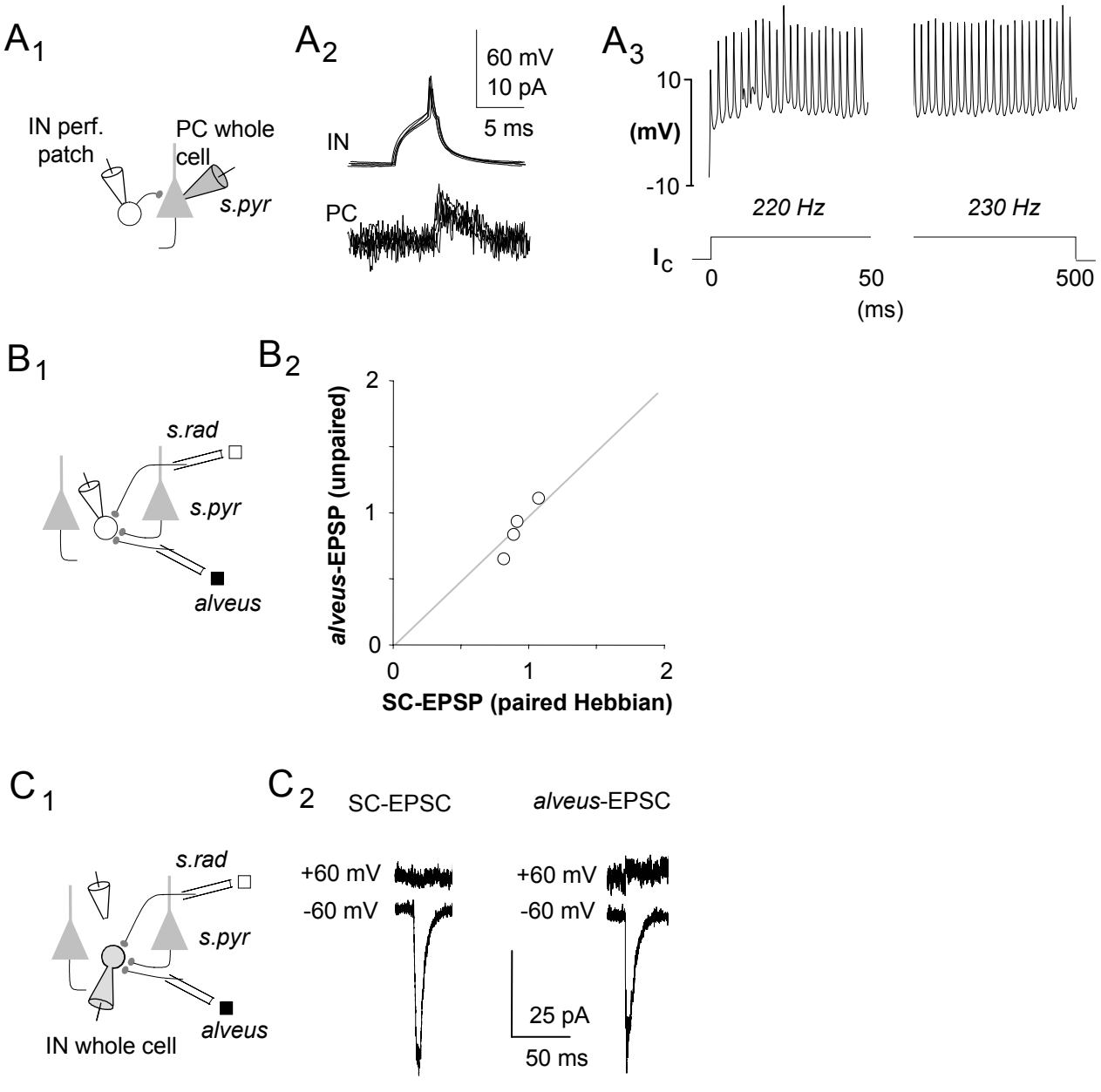

Lamsa *et al*. Fig. S7

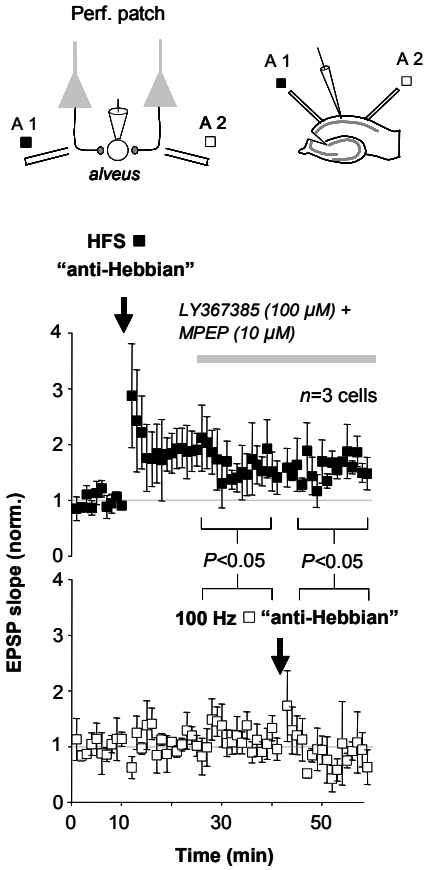

Lamsa *et al*. Fig. S8